Erik Johnson[a,b], Sergei Prokofjev[a,c], Victor Zhilin[a,c], Ulrich Dahmen[d]
[a] Nano Science Center, Niels Bohr Institute, University of Copenhagen, Denmark
[b] Materials Research Dept., RISØ National Laboratory, Denmark
[c] Institute of Solid State Physics, Chernogolovka, Russia
[d] National Center for Electron Microscopy, LBNL, Berkeley, USA

Diffusional behavior of nanoscale lead inclusions in crystalline aluminum

Dedicated to Professor Dr. Lasar Shvindlerman on the occasion of his 70th birthday

In-situ transmission electron microscopy (TEM) observations reveal a permanent chaotic motion of nanosized liquid Pb inclusions embedded in thin aluminum foils. Individual trajectories of the inclusions were analysed to determine the character of their motion. The inclusions moving freely inside a crystal display motion with three-dimensional random walk characteristics while inclusions attached to dislocations display spatially confined random motion localized to the close vicinity of the dislocation lines. The diffusion coefficients of inclusions moving freely in the matrix were determined using Einstein's classical equation for diffusion of Brownian particles. The diffusion coefficients of inclusions trapped on dislocations were found using an equation based on Smoluchowski's analysis of Brownian motion of a particle under the action of a linear elastic restoring force. The dependence of the diffusivity on the size of the inclusions suggests that their mobility is controlled by kinetic processes on the inclusion/matrix interfaces. The Arrhenius analysis exhibits two regions with different temperature dependencies. We suppose that this is related to the existence of {111} facets on the inclusion/matrix interfaces.

Keywords: Transmission electron microscopy; Nanoscale lead inclusions in solid aluminum; Random motion; Effect of dislocations; Effect of temperature and size on diffusion coefficient

1. Introduction

It is well-known, that the mobility of pores, gas bubbles, and liquid and solid inclusions in solid multiphase materials held at elevated temperature has a strong impact on the rate of evolution of the microstructure of materials and, thus, on their lifetime [1]. This is clearly demonstrated for noble gas bubbles in reactor materials [1, 2]. A high mobility of second phase inclusions may control the kinetics of high-temperature creep in dispersion-hardened alloys and the kinetics of recrystallization [1]. For example, the influence of second phase particles on the rate of migration of grain boundaries has been shown theoretically and in experimental studies, where anomalous grain boundary migration was observed in Al-rich Al–Pb alloys containing liquid Pb inclusions [3]. In addition, a strong destructive effect of pores and second phase inclusions is expected in circuits of modern nanodevices [4, 5]. These examples indicate the importance of basic investigations on the behavior of bubbles, inclusions, pores, etc. in solid matrices, e. g. studies of:

1. The mechanisms controlling their mobility;
2. The effect of their structure and morphology on their mobility;
3. The influence of microstructure elements such as dislocations, grain and interphase boundaries, on their kinetic behavior.

In the present paper the results of our *in-situ* TEM studies of the kinetic behavior of nanoscale liquid Pb inclusions in thin aluminum foils are described. In these studies the motion of free inclusions as well as inclusions attached to dislocations is investigated. "Pb inclusions in Al" is an extremely good model system for studying the motion of inclusions in a solid matrix 1) because the extremely good electron-microscopy contrast of Pb inclusions in Al allows precise investigations of their morphology and structure [6–8], 2) because the low melting point of lead and the low miscibility between liquid lead and solid aluminum means that the liquid lead inclusions are chemically inert, and to a first approximation may be considered as individual confined systems, and 3) because the high mobility of liquid Pb inclusions in Al gives the possibility to conduct quantitative *in-situ* TEM studies of their motion and to observe the influence of matrix defects on their motion [9–13].

2. Experimental procedure

The samples used in our studies were prepared from ribbons of alloys of Al with about 1 at.% Pb. They were obtained by rapid solidification from a temperature above the Al–Pb liquid immiscibility gap (Fig. 1) by melt spinning technique. A stabilized microstructure of the samples consisting of nanosized Pb inclusions in the polycrystalline Al matrix was obtained by a subsequent annealing in an Ar atmosphere.

In-situ TEM studies of diffusion of the inclusions were carried out in a 200 kV Phillips CM 20 microscope using a single tilt heating stage (Gatan). The observations were recorded on video with a velocity of 25 frames per second. Coordinates of the positions of centers of individual inclu-

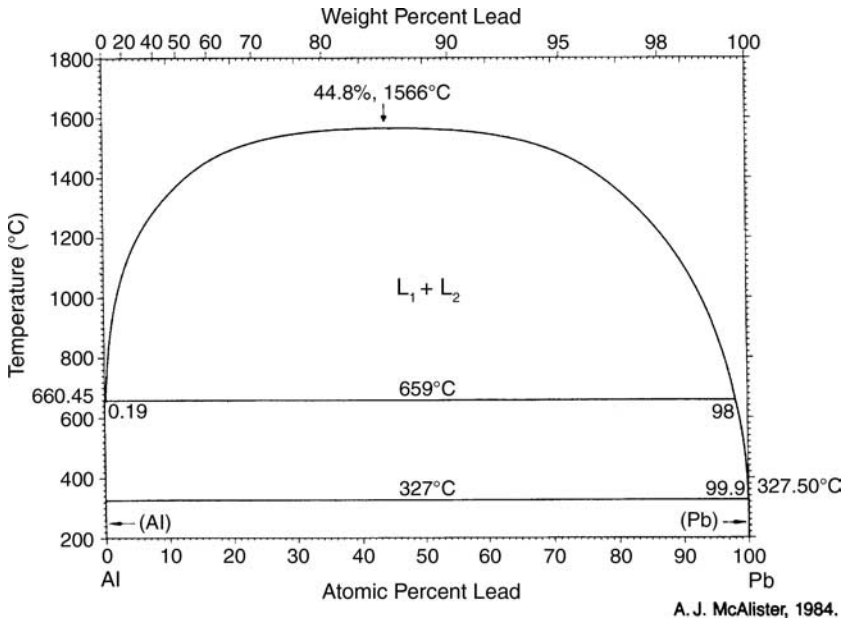

Fig. 1. Al–Pb phase diagram [14].

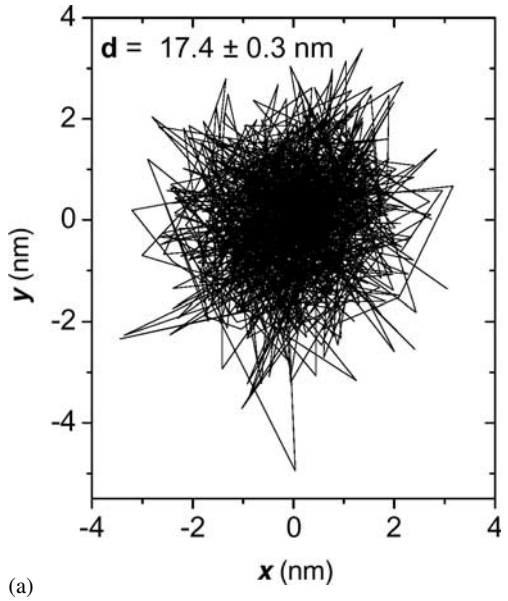

(a)

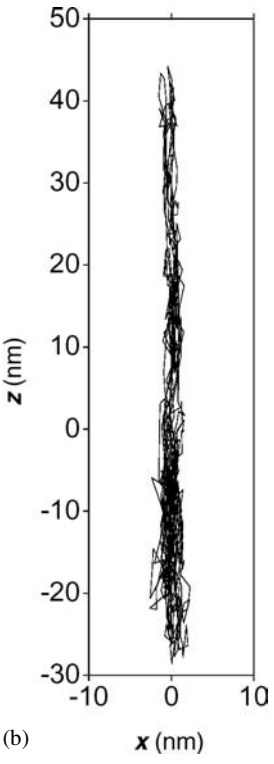

(b)

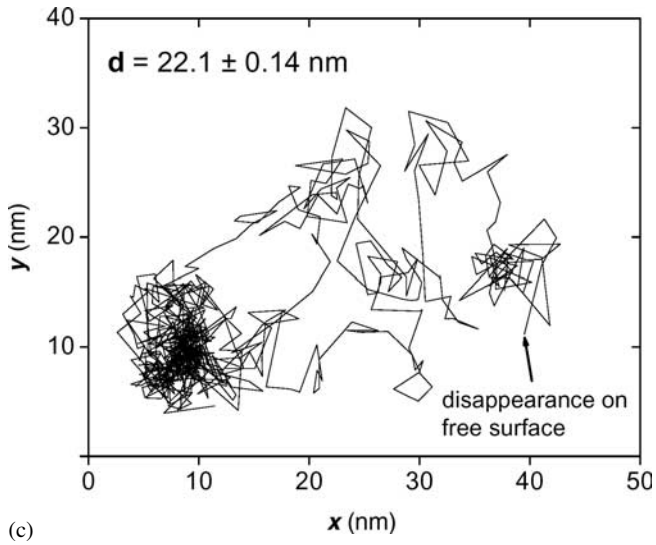

(c)

Fig. 2. Trajectories of trapped Pb inclusions (a) in the transverse plane, and (b) along the dislocation line. (c) Trajectory of a Pb inclusion initially trapped, and, then, moving freely after breakaway. After [13].

sions were obtained from frame-by-frame measurements on digitized images. Points of trajectories of individual inclusions were obtained by subsequent correction for sample drift during the observations. The diameters d of all inclusions have been measured as well. The accuracy of the relative changes in sample temperature is estimated to be around 1 K, while the error in the absolute value of the temperature determination is regarded as to be around 5 K.

3. Kinetic behaviour of inclusions attached to dislocations

TEM observations show that a large fraction of the inclusions are attached to defects – quenched-in dislocations and grain boundaries. Trajectories of inclusions connected with dislocations are localized to the vicinity of the dislocation lines. Their shape depends on the orientation of the dislocations relatively the image plane. Thus, in Fig. 2a the dislocation is oriented along the normal to the image plane, and in Fig. 2b the dislocation is inclined. Sometimes a trapped inclusion is seen to detach from the dislocation and move freely for relatively short time until it either disappears at a free surface of the foil, coalesces with another inclusion, or becomes re-trapped by another defect. Figure 2c shows the trajectory of such an inclusion. Initially the trajectory is localized and after breakaway it becomes non-localized until the inclusion finally disappears at the free surface.

Figure 3a shows a set of two inclusions with diameters of 14 nm and 15 nm respectively attached to one dislocation, which is out of contrast in the micrograph. Their motion was observed at 720 K. Indeed, the trajectories of the inclusions as a whole displayed in Fig. 3b overlap partially in space but not in time, and hence coalescence of the inclusions was not observed during an observation time of around 10 minutes.

The trajectories of inclusions attached to dislocations suggest that their movements are random oscillations with small amplitudes in a plane perpendicular to the dislocation line and with large amplitudes along the dislocation, Figs. 2a, b and Fig. 3b. This is indicated clearly by the time

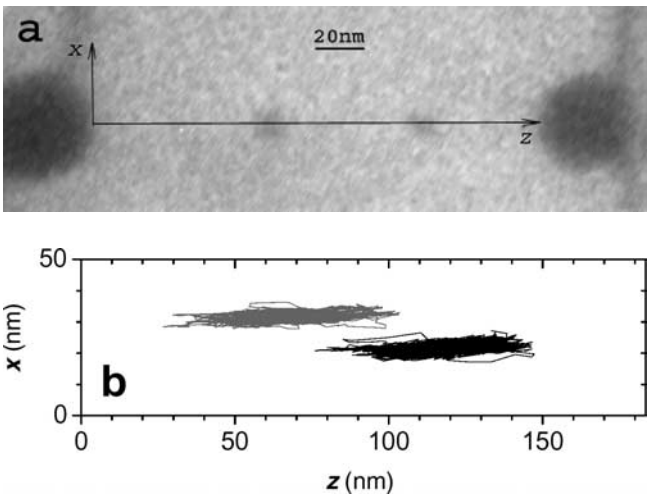

Fig. 3. (a) TEM micrograph of the system of two inclusions trapped on one dislocation. The Z-axis lies along the invisible dislocation line. (b) The trajectories of the inclusions. For better visibility the two traces are shifted relative to each other along X-axis.

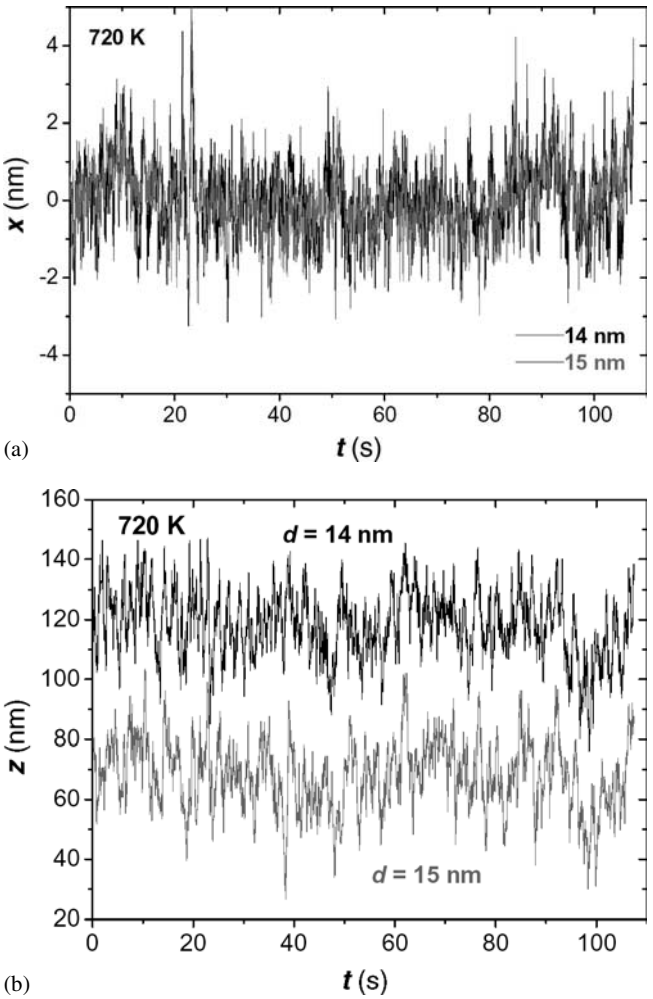

Fig. 4. The time dependence of (a) transverse and (b) longitudinal displacements of the two inclusions shown in Fig. 3a for the 110 s long observation. The traces depict random oscillatory behavior. After [11].

dependencies of their transverse displacements (Fig. 4a) and longitudinal displacements along dislocation line (Fig. 4b). The distributions of the x- and z-displacements in the transverse and longitudinal movements respectively are close to the Gaussians (Fig. 5a, b) that correspond to spatially confined random motion. The standard deviations of the oscillations of 14 nm and 15 nm inclusions are $\sigma_x = 1.04$ nm and $\sigma_y = 0.89$ nm in the transverse plane, and $\sigma_z = 11.3$ nm and $\sigma_z = 11.9$ nm along the dislocation, respectively. These confinements are not purely geometrical as, for example, a random motion of a particle between two elastically reflecting walls (square potential well) since in the latter case we should obtain a rectangular distribution of displacements [15].

In order to study the motion of inclusions in the transversal plane the ensemble of inclusions presented in Fig. 6 was used, as most of them displayed trajectories similar to the one shown in Fig. 2a. They were investigated at 720 K. The inclusions marked by the white circles in Fig. 6a had broken away from their dislocations to move freely along non-localized trajectories. They were used to study free random motion.

Figure 7 demonstrates again that x- and y-components of transverse oscillations of trapped inclusions are close to Gaussian distributions with similar standard deviations of

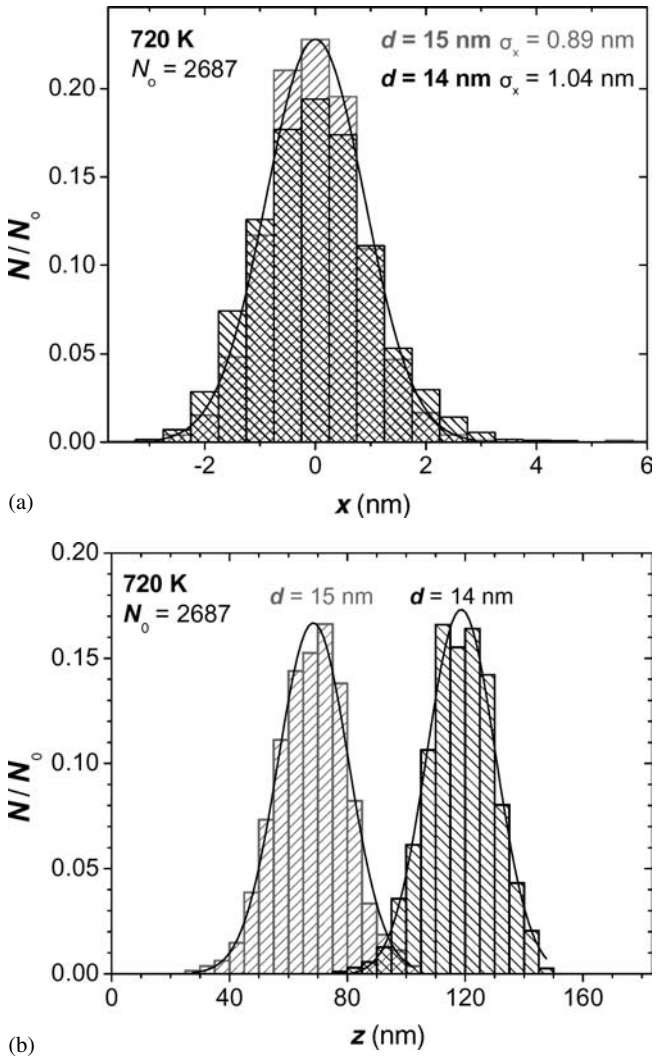

Fig. 5. (a) Probability distributions of positions of the inclusions in the direction of *X*-axis perpendicular to the dislocation line. The close-to-Gaussian shapes are due to the elastic action of dislocation on the inclusions. (b) Probability distributions of positions of the inclusions along the dislocation line. Their close-to-Gaussian shapes are due to mutual repulsion of the inclusions and their repulsion from the fixed ends of the dislocation. The ends of the *Z*-axis segment correspond to the ends of the dislocation.

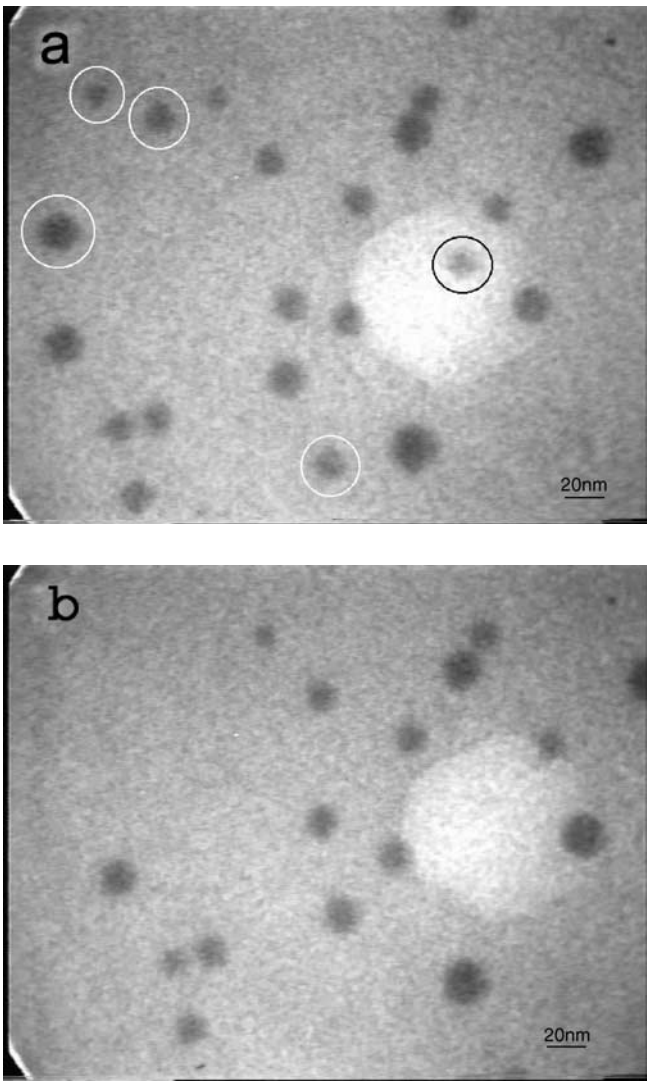

Fig. 6. TEM micrographs of the foil area studied. (a) The first and (b) the last frames from the analyzed video sequence. The inclusions marked in frame (a) broke away from their dislocations to move freely and disappear on the surfaces of the foil after a short time. They are absent in frame (b). The large bright spot in the frames is a thinner and possibly oxidized area of the foil.

σ_x = 1.08 nm and σ_y = 1.17 nm. It indicates that the two-dimensional distribution of transverse oscillations have an axial symmetry. This is confirmed by the trajectory shown in Fig. 2a. Within the experimental error the standard deviation $\sigma_\rho = (\sigma_X^2 + \sigma_Y^2)^{1/2}$ does not depend on the size of the inclusions (Fig. 8). Since in the present case the pinning dislocations are expected to be edge-on and identical, Fig. 8 suggests that the magnitude of σ_ρ is controlled by the dislocation characteristics rather than by the size of inclusion. For the 14 inclusions used in Fig. 6 the average of σ_ρ is equal to 1.15 nm.

4. Model for effect of dislocation on motion of inclusion

The above analysis suggests that a fixed dislocation will act as an elastic string, returning the inclusions to their equilibrium positions defined by the conditions where the dislocation has its minimal length. This model is shown schematically in Fig. 9, which shows an inclusion P attached to the

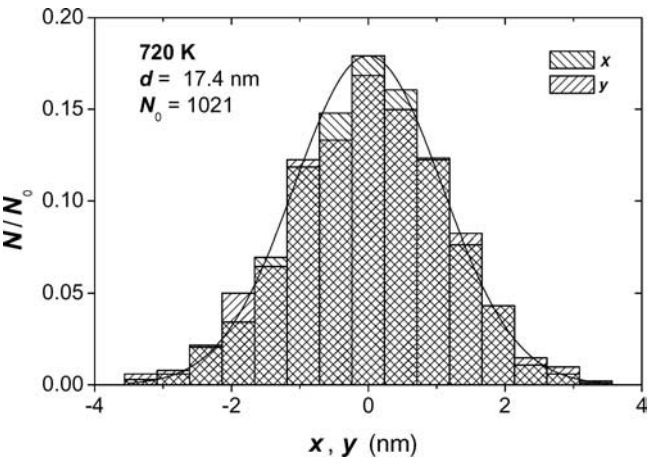

Fig. 7. Probability distributions of *x* and *y* of one of the trapped inclusions shown in Fig. 6. The solid line is a Gaussian fit. N_o is the total number of measurements. After [13].

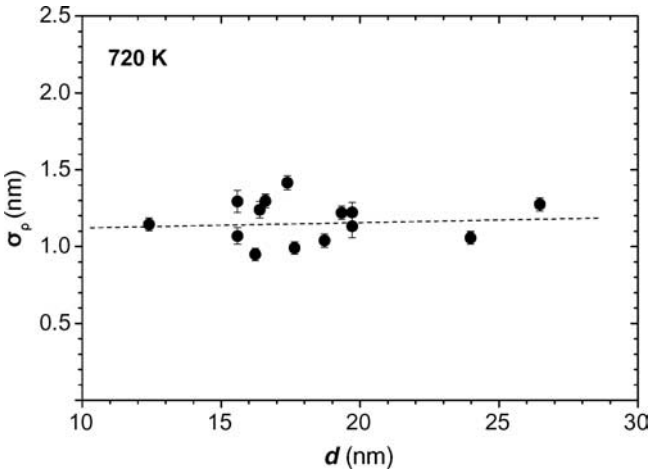

Fig. 8. Dependence of σ_ρ of the inclusions trapped by the dislocations shown in Fig. 6 on their diameter. The dashed line fits the experimental points. Its slope is zero within the error. The average σ_ρ = 1.15 nm.

dislocation segment of length 2*L*, whose fixed ends "$-L$" and "L" lie on the *Z*-axis.

Here ρ is the displacement of the inclusion from the straight dislocation geometry and z determines its distance from the midpoint 0 of the dislocation segment. The arrow $\boldsymbol{F}$ in this figure shows the restoring force due to the elasticity of the dislocation. A projection of the force on the *Z*-axis causes the repulsion of the inclusion from the closer fixed end of the dislocation ('*L*' in Fig. 9).

Using the above model, the random oscillations of trapped inclusions can be analyzed as a random walk under the action of an elastic force. The problem of one-dimensional Brownian motion of a particle under action of a restoring force $P = -f \cdot x$ (f is the force constant) was analyzed by Smoluchowski [15]. He showed that the stationary distribution of the deviation of the particle from its equilibrium position $x = 0$ is Gaussian with a standard deviation $\sigma_x = (kT/f)^{1/2}$, where k is the Boltzmann constant, and T is the temperature. Then, in the case of central symmetry ($f_x = f_y$) the distribution of $\rho = \sqrt{x^2 + y^2}$ is Gaussian with the standard deviation $\sigma_\rho = (2kT/f)^{1/2}$.

Generally speaking, the motion of inclusions attached to dislocations is a three-dimensional problem. However, the assumption of axial symmetry reduces this problem to a two-dimensional one. In contrast to Smoluchowski's model, in the case of motion of an inclusion attached to a dislocation the restoring force is not linear, and, the force constant is a function of ρ and z. The displacement of an inclusion to a point $P(\rho, z)$ causes an elongation of the dislocation line

$$\Delta L = \sqrt{(L+z)^2 + \rho^2} + \sqrt{(L-z)^2 + \rho^2} - 2L \qquad (1)$$

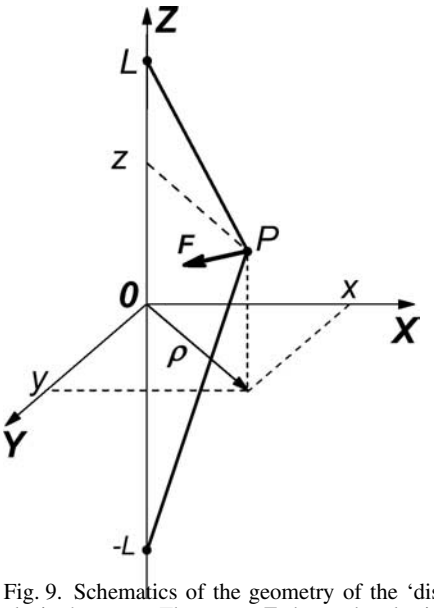

Fig. 9. Schematics of the geometry of the 'dislocation – attached inclusion' system. The arrow $\boldsymbol{F}$ shows the elastic restoring force acting on the attached inclusion *P*, which is due to the elasticity of the dislocation.

which increases the elastic energy of the system by $\Delta U = U_0 \Delta L$, where U_0 is the energy of the unit dislocation. The function $\Delta U = \Delta U(\rho, z)$ determines the elastic energy field. Then, the elastic restoring force acting on the inclusion is $\boldsymbol{F} = -\mathrm{grad}(\Delta U)$ or assuming an axial symmetry $\boldsymbol{F} = -\dfrac{\partial \Delta U}{\partial \rho}\dfrac{\boldsymbol{\rho}}{\rho} - \dfrac{\partial \Delta U}{\partial z}\dfrac{\boldsymbol{z}}{z}$. The force can be written as $\boldsymbol{F} = -f_\rho \boldsymbol{\rho} - f_z \boldsymbol{z}$, where $f_\rho = f_\rho(\rho, z)$ and $f_z = f_z(\rho, z)$ are the force constants for the inclusion motion perpendicular and parallel to *Z*-axis, respectively. They are $f_\rho = \dfrac{1}{\rho}\dfrac{\partial \Delta U}{\partial \rho}$ and $f_z = \dfrac{1}{z}\dfrac{\partial \Delta U}{\partial z}$. The expressions for f_ρ and f_z can be obtained assuming that $(\rho/L)^2 \ll 1$, which is a good approximation as it is suggested by Fig. 2b and Fig. 3b.

$$f_\rho \cong \frac{2U_0}{L}\frac{1}{(1-\lambda^2)} \quad \text{and} \quad f_z \cong \frac{2U_0}{L}\frac{\rho^2}{L^2(1-\lambda^2)^2} \qquad (2)$$

where $\lambda = z/L$ [16]. Since $L/\rho \sim 100$, so $f_z \ll f_\rho$. In this case the transverse (ρ) motion is much faster than the z-motion along the dislocation and we can use the adiabatic approximation for the longitudinal motion in comparison with the transverse motion. So after averaging over transverse oscillations the motion of the particle is reduced to one-dimensional longitudinal motion. It can be shown analytically in the same approximation that the density of the steady-state

Table 1. Comparison of experimental values of the root mean squared displacements σ_ρ and σ_z with the theoretic calculations.

Data source	L (nm)	σ_ρ (nm)		σ_z (nm)		σ_ρ/σ_z	
		Exper.	$(4kTL/5U_o)^{1/2}$	Exper.	$L/\sqrt{5}$	Exper.	$(4kT/U_oL)^{1/2}$
Fig. 8	100*	1.15	0.99	–	44.7	–	$2.22 \cdot 10^{-2}$
Fig. 5, 15nm	~60	1.26**	0.77	11.9	26.8	0.11	$2.86 \cdot 10^{-2}$
Fig. 5, 14nm	~60	1.47**	0.77	11.3	26.8	0.13	$2.86 \cdot 10^{-2}$
***	93	0.83**	0.96	10.5	41.6	$7.9 \cdot 10^{-2}$	$2.30 \cdot 10^{-2}$

* half the foil thickness assumed; ** $\sigma_\rho = \sqrt{2}\,\sigma_x$, *** the attached inclusion at 722 K [17]

probability distribution of λ is [16]:

$$w(\lambda) = {}^3/_4(1-\lambda^2) \quad (3)$$

Using Eq. (3) we obtain $\sigma_\lambda^2 = 1/5$, where σ_λ is the root mean squared value of λ [16]. It is interesting, that an analysis of one-dimensional random motion of free particle between two elastically reflecting walls spaced by $2L$ gives $\sigma_\lambda^2 = 1/3$ [15]. According to the law of equipartition of kinetic energy and accounting for harmonic oscillatory motion in the transverse plane (Eq. (2)) we have equivalence of kinetic and potential energy. Hence

$$f_\rho^* \sigma_\rho^2/2 = f_\rho^*(\sigma_x^2 + \sigma_y^2)/2 = kT/2 + kT/2 = kT \quad (4)$$

where σ_ρ is the root mean square value of ρ. Using Eqs. (2–4) one can obtain the expressions for average force constants of the transverse and longitudinal oscillations given by $f_\rho^* = \dfrac{3U_0}{L}$ and $f_z^* = \dfrac{3k\mathrm{T}}{L^2}$, respectively. Thus, f_ρ^* is determined by the elasticity of the dislocation, and f_z^* is governed by the energy of thermal motion. For the mean square displacements in the transverse and longitudinal movements we finally get $\sigma_\rho^2 = 4kTL/5U_0$, $\sigma_z^2 = L^2/5$ and $(\sigma_\rho/\sigma_z)^2 = 4kT/U_0L$. Since the elastic energy of the dislocation U_0L is much larger than the thermal energy kT, the trajectories of inclusions attached to dislocations are elongated in the direction of the dislocation line. The inclusion size has no effect on either f_ρ^* and f_z^*, or on σ_ρ and σ_z in agreement with the results in Fig. 8. In Table 1, and σ_z determined from the experimental data in Fig. 5 and Fig. 7, are compared to the values estimated from the elastic model. In the calculations we have used $U_0 \sim \mu b^2/2$, where μ is the shear modulus and b is the Burgers vector. Here $\mu = 19.7$ GPa is calculated using the expression $\mu = (c_{11} - c_{12} + 3c_{44})/5$ [18] with the elastic moduli c_{11}, c_{12} and c_{44} for Al crystals at 720 K obtained by linear interpolation of data obtained by Gerlich and Fisher [19]. In fcc metals $b = a/\sqrt{2}$, where a is the lattice constant equal to 0.405 nm for Al [20]. Other parameters used in the calculations are given in Table 1. One can see that the theoretical estimates of σ_ρ and σ_z agree reasonably with their values determined from the experimental data. The larger discrepancy in σ_z may be caused by the stronger repulsion of Pb inclusions from the ends of the dislocations than in the framework of the elastic model, where the real situation may be somewhat simplified. Nevertheless, the comparison carried out in Table 1 in general supports the elastic model accepted for description of the motion of the trapped Pb inclusions.

For one-dimensional motion of a Brownian particle under action of a linear restoring force Smoluchowski had obtained the dependence of the mean squared displacement of the particle $<\Delta x^2>$ from its initial position as a function of elapsed time Δt [21]:

$$<\Delta x^2> = 2\sigma_x^2[1 - \exp(-D_\mathrm{p}\Delta t/\sigma_x^2)] \quad (5)$$

The average is taken over the trajectory. As above $\sigma_x = (kT/f)^{1/2}$, and D_p is the diffusion coefficient of the particle. Here D_p can be determined from Eq. (5) if the particle trajectory is recorded with the time steps small enough to obey the relation $D_p\Delta t/\sigma_x^2 \leq 1$. At $D_p\Delta t/\sigma_x^2 \ll 1$ this equation is transformed to Einstein's equation for one-dimensional diffusion [22]. In the two-dimensional central symmetric case ($\sigma_x = \sigma_y$) the equation analogous to Eq. (5) is

$$<\Delta\rho^2> = 2\sigma_\rho^2[1 - \exp(-2D_\mathrm{p}\Delta t/\sigma_\rho^2)] \quad (6)$$

Here $<\Delta\rho^2> = <\Delta x^2> + <\Delta y^2>$ is the mean squared displacement, and $\sigma_\rho^2 = 2\sigma_x^2$.

In the following we will apply Eq. (5) and Eq. (6) to determine the diffusion coefficients of inclusions attached to dislocations using the data on their longitudinal and transverse motion, respectively. Of course, in this case the σ_ρ and σ_x are parameters, whose meanings differ from those in Smoluchowski's model.

5. Mobility of liquid Pb inclusions in aluminum

5.1. Free inclusions

In Fig. 10 the dependence $\sqrt{<\Delta\rho^2>}$ versus t is plotted in log–log coordinates for the inclusion (~ 17 nm) before (curve 2) and after (curve 1) its breakaway from the dislocation at the temperature of 720 K. Here $<\Delta\rho^2> = <\Delta x^2> + <\Delta y^2>$, where $\Delta\rho$ is the projection of the displacement of the inclusion during the elapsed time Δt onto the XY image plane, and Δx and Δy are the projections of $\Delta\rho$ on the X- and Y-axes, respectively. The averages are taken over the trajectory of the inclusion. Curve 1 is fitted well with Einstein's equation [22]

$$D_\mathrm{p} = <\Delta\rho^2>/4\Delta t \quad (7)$$

shown by the dashed straight line in Fig. 10. This confirms the free random motion of the inclusion. According to the fitting procedure the diffusion coefficient is equal to $1.09 \cdot 10^{-16}\ \mathrm{m^2 s^{-1}}$. Curve 2 is the transverse motion of the same inclusion before its detachment from the dislocation fitted with the Smoluchowski equation (Eq. (6)), and although the movement on the time scale that we can record, is spatially confined, the small-time extension of the curve is nearly parallel to curve 1 for the free particle. The diffusion coefficient obtained from the Smoluchowski fit is $0.72 \cdot 10^{-16}\ \mathrm{m^2 s^{-1}}$ that is fairly close to the value for the free movement. The non-monotonous behavior of the curves in Fig. 10 and Fig. 12 at larger values of Δt is due to geometrical constraints of the paths and poor statistics.

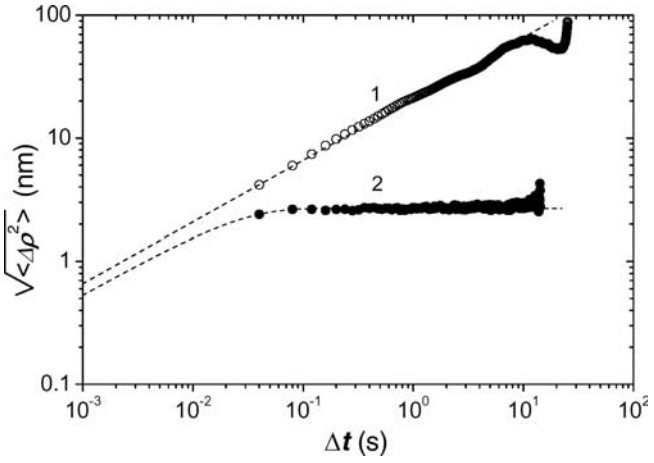

Fig. 10. Root mean squared ρ-displacement of the 17 nm inclusion in the free (curve 1) and the trapped (curve 2) states as a function of elapsed time. The dashed straight lines show the fitting of curve 1 with Einstein's equation and curve 2 by Eq. (6). After [13].

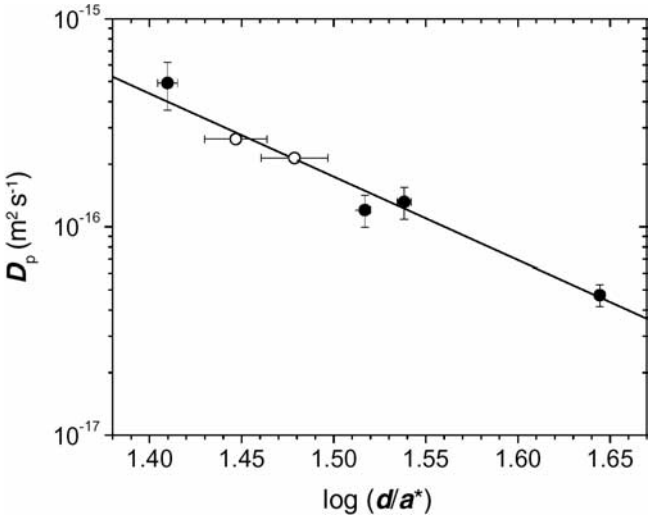

Fig. 11. Diffusion coefficient of free inclusions (solid circles) and of the longitudinal motion of the 14 nm and 15 nm trapped inclusions (open circles) as a function of their diameter. The solid line fits the free motion data points by Eq. (9). After [13].

The dependence of the diffusion coefficient D_p of free inclusions (the solid circles) on their diameter d is shown in log–log coordinates in Fig. 11. The linear fitting gives a slope of -4.0 ± 0.5. The inclusion inside the bright area in Fig. 6, which is a thinner and possibly oxidized region of the foil (it is marked by the black circle in Fig. 6a) is not included in the analysis, as this inclusion depicted anomalously slow mobility.

5.2. Motion of attached inclusions along dislocation.

Figure 12 shows the experimental results of the root mean square longitudinal displacements of the 14 nm and 15 nm inclusions (Fig. 3a) $\sqrt{<\Delta z^2>}$ as a function of elapsed time Δt at 720 K plotted in log–log coordinates. Both curves have slopes close to $^1/_2$ at small Δt indicating free random motion of the inclusions. In contrast, at larger Δt the mean square displacements become independent of Δt and approach constant values as they should for confined random motion pattern.

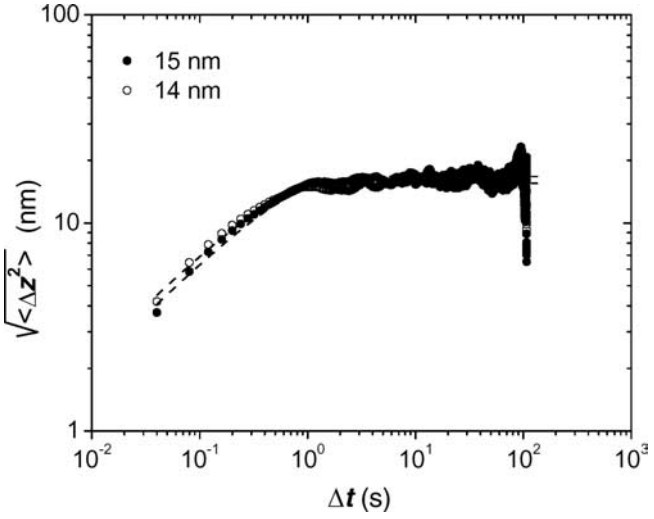

Fig. 12. Root mean squared longitudinal displacement of 14 nm and 15 nm inclusions at 720 K as a function of elapsed time. The dashed lines are the fits to Eq. (5).

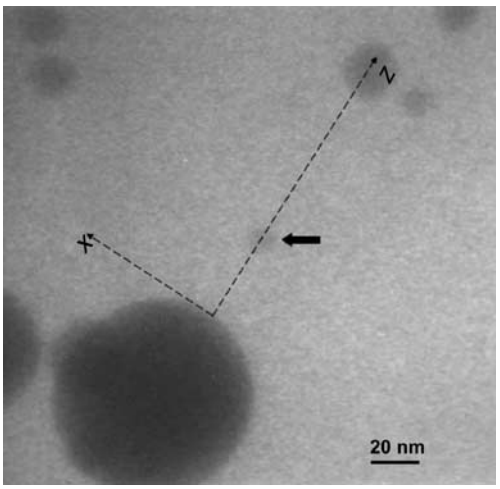

Fig. 13. Video frame showing micrograph of the 12 nm inclusion (shown by the arrow) attached to the invisible dislocation lying along Z-axis. Its ends are fixed by the two larger inclusions.

The fitting results give values for the diffusion coefficients of $D_p = 2.64 \cdot 10^{-16}\,m^2 s^{-1}$ and $D_p = 2.14 \cdot 10^{-16}\,m^2 s^{-1}$ for 14 nm and 15 nm inclusions, respectively. They agree with the size dependence of the diffusivities of free inclusions, Fig. 11 (open circles). Thus, the effect of the dislocation on the longitudinal mobility of the trapped inclusions is not strong. It also indicates that the microscopic mechanism controlling the mobility of free and trapped inclusions is likely to be the same.

5.3. Effect of temperature on mobility

The longitudinal motion of an inclusion with a size of 12 nm was used to study the effect of temperature on the diffusion coefficient. The inclusion is shown by the arrow in Fig. 13. In this experiment the temperature was stepped down in the range from 688 to 622 K and the movement of the inclusion was observed for ten different temperatures. Figure 14 presents the longitudinal displacements of the inclusion as a function of time at different temperatures. The amplitude of the oscillations diminishes as the temperature goes down. The diffusion coefficients of the inclusion were determined using Eq. (5). The Arrhenius plot of the diffusion coefficient (Fig. 15) is non-linear. It can, however, be

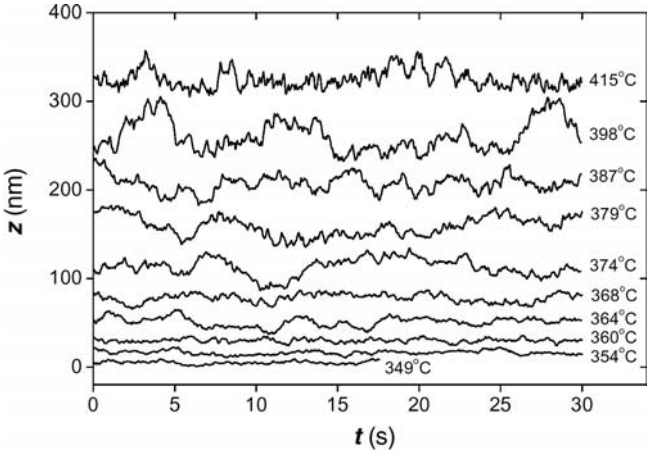

Fig. 14. The time dependences of longitudinal displacements of the 12 nm inclusion at different temperatures.

fitted to two linear segments representing two temperature regions characterized by different activation enthalpies. The low-temperature activation enthalpy is equal to 3.05 ± 0.15 eV while the high-temperature value is 1.60 ± 0.23 eV. The transition zone is around 650 K.

6. Discussion of the mechanisms of mobility

According to the Al–Pb phase diagram [14] (Fig. 1) a saturated solid solution of Pb in Al and a saturated liquid solution of Al in Pb are in equilibrium at the surface of the inclusions. However, thermal and concentration fluctuations can give rise to local growth and dissolution of matrix crystal at the surface of the inclusions, i. e. causing local displacements of the inclusion/matrix interface. It is natural to suppose that this may lead to net shifts of the centers of the inclusions, and, consequently, to their motion. Motion of inclusions in the crystalline matrix is necessarily related to local destruction of the crystal lattice in the direction of the motion, and its creation at the opposite side. Thus, the displacement of an inclusion is accompanied by detachment of atoms from the matrix crystal, their consequent transfer and rejoining to the crystal lattice.

The rate of the dissolution – growth process V of a crystal can be described for small enough supersaturation Δc of solution near the crystal surface by the following equation [23]

$$V = \Delta c \beta / (1 + \delta \beta / D) \tag{8}$$

Here β is the kinetic coefficient of crystallization, D is the coefficient of atomic diffusion controlling the mass transfer, and δ is the width of diffusion boundary layer near the crystal surface. Eq. (8) shows that the rate is controlled by diffusion (the diffusion regime) if $\delta\beta/D \gg 1$, and by crystal growth-dissolution at the crystal-solution interface (the kinetic regime) if $\delta\beta/D \ll 1$. A sign of Δc determines whether growth or dissolution of the crystal takes place.

6.1. The diffusion control of mobility.

In the diffusion regime the mobility of the Pb inclusions in Al can be controlled by diffusion of Al through the liquid Pb inclusion, diffusion of Pb through the Al matrix, and diffusion of Al along the interface of the inclusion. The different mechanisms will correspond to different size dependencies of the diffusivity of the inclusions [24, 25]:

$D_p \sim d^{-2}$ for diffusion through inclusion;
$D_p \sim d^{-3}$ for diffusion through matrix;
$D_p \sim d^{-4}$ for interfacial diffusion.

The dependence $D_p \sim d^{-4}$ found for liquid Pb inclusions in Al (Fig. 11) indicates that in the diffusion regime their mobility is controlled by diffusion along the Pb/Al interface. The interfacial diffusion coefficient D_{int} is estimated by fitting of the experimental data using the relationship of Nichols [25], which is adapted to the case of liquid fcc metal inclusions,

$$D_p = (6/\sqrt{2}\pi)\,(d/a^*)^{-4}\, cD_{int} \tag{9}$$

The atomic size is set by the expression $a^* = (1 + \gamma)^{1/3}\, a$, where $\gamma = 0.035$ is the relative volume increase during melting of lead, and $a = 0.495$ nm is the lattice constant of solid lead [20]. The parameter c in Eq. (9) is the interfacial concentration of atoms participating in the diffusion. Assuming $c = 1$ the fitting by Eq. (9) (dashed straight line in Fig. 11) gives $D_{int} = (1.29 \pm 0.16) \cdot 10^{-10}\ m^2 s^{-1}$ at 720 K. Application of Eq. (9) to the data of Fig. 15 gives the values for the pre-exponents of D_{int}: $(D_{int})_o = 23.3\ m^2 s^{-1}$ for the high-temperature region and $(D_{int})_o = 4.36 \cdot 10^{12}\ m^2 s^{-1}$ for the low-temperature region.

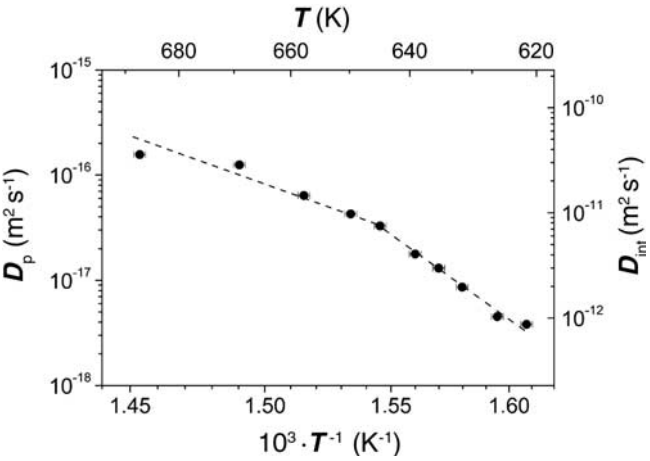

Fig. 15. Arrhenius plot of the diffusion coefficient obtained for longitudinal motion of 12 nm trapped inclusion. The standard errors of D_p are less than the size of the data points markers. D_{in} is the coefficient of interfacial diffusion obtained with Eq. (9).

Unfortunately, data for diffusion on the Al surface are not available. Instead, we use the empirical equation $D_s = 7.4 \cdot 10^{-2} \exp(-30 T_m/T)\ m^2 s^{-1}$, which was proposed by Gjostein for surface self-diffusion in fcc metals at $T > 0.77 T_m$ [26]. This equation gives the activation enthalpy of surface self-diffusion, which numerically is equal to $30 T_m$ kcal/mol. The latter is about of 1.2 eV for Al, that is comparable with 1.60 eV obtained by us for the high-temperature region. Also this equation gives $D_s = 2.3 \cdot 10^{-10}\ m^2 s^{-1}$ in Al at 720 K comparable with $D_{int} = 1.29 \cdot 10^{-10}\ m^2 s^{-1}$ obtained by us. The values of D_{int} obtained with Eq. (9) using the data of Fig. 15 are in a reasonable agreement with D_s as well. Thus, we conclude that in the high-temperature region diffusion along the Al/Pb interface may be the mechanism controlling the mobility of Pb inclusions.

The low-temperature activation enthalpy 3.05 eV exceeds significantly those of atomic diffusion mechanisms possible in the Al–Pb system (1.5 eV for bulk diffusion of Pb in Al [27]). This indicates that dissolution of Al matrix at the interface rather than diffusion may govern the mobility of the inclusions in the low-temperature region. Actually, the pre-exponential factors, especially the one $(4.36 \cdot 10^{12} m^2 s^{-1})$ obtained for the low-temperature region, are many orders of magnitude larger than the pre-exponential factors typical for diffusion [28].

6.2. The dissolution kinetics control of mobility.

In the kinetic regime an activation enthalpy ΔH can be related roughly to the energy of detachment of an Al atom from the free surface of an Al crystal. In the framework of a nearest neighbor model with pair interactions, $\Delta H = Z\varepsilon/2$, where Z is the number of nearest neighbours of the atom, which breaks away, and ε is the interatomic bond energy.

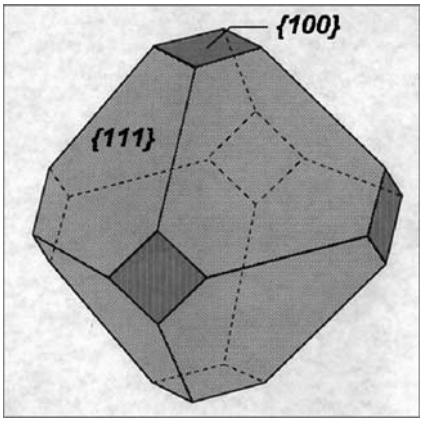

(a)

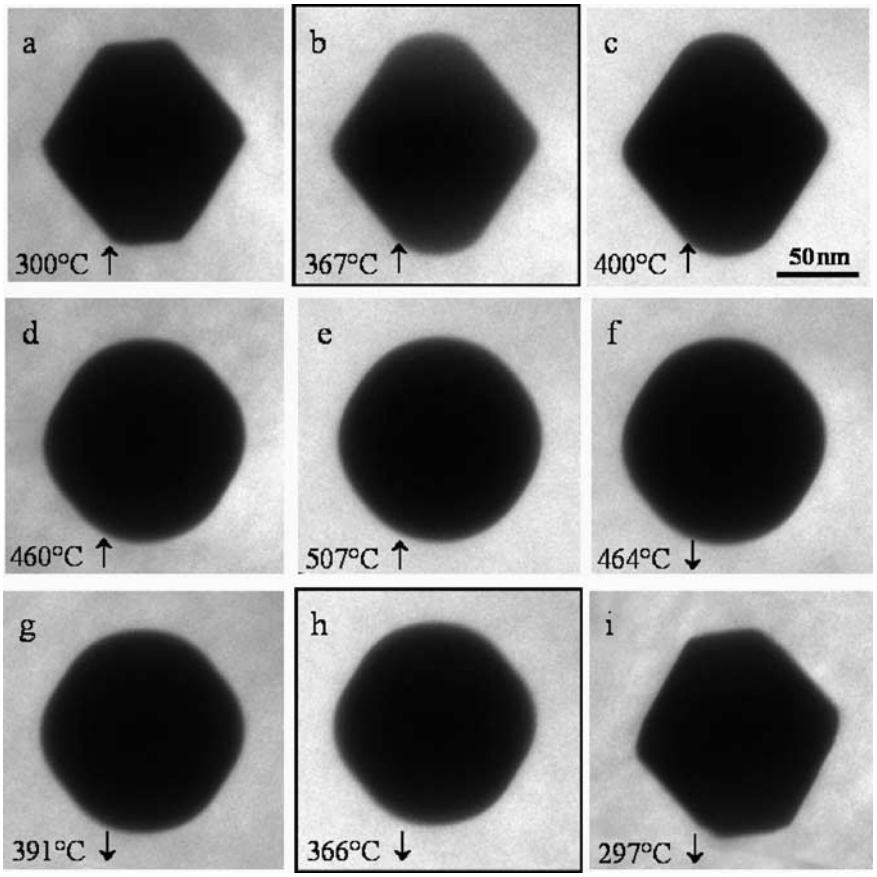

(b)

Fig. 16. (a) The shape of solid Pb inclusion in Al [6]. (b) Effect of temperature on shape of the Pb inclusion in Al [7].

This can be estimated as $2\Delta H_s/Z_o$, where ΔH_s is the sublimation enthalpy (3.36 eV for Al [20]), and Z_o is the coordination number (= 12 for fcc lattice). Then, $Z = Z_o(\Delta H/\Delta H_s)$. An account of the energy balance of dissolution of the detached Al atom in the Pb melt gives $\Delta H = (Z/Z_o)\,\Delta H_s + \Delta H_{mix}$, where ΔH_{mix} is the enthalpy of mixing in Al–Pb solutions (0.37 eV), which is obtained from the Al partial free energy of mixing in the Pb-rich liquid given in [14]. Therefore,

$$Z = Z_o[(\Delta H - \Delta H_{mix})/\Delta H_s] \qquad (10)$$

Equation (10) gives $Z = 9.6$ for the low-temperature region ($\Delta H = 3.05$ eV), and $Z = 4.4$ for the high-temperature region ($\Delta H = 1.60$ eV). The number of nearest neighbors of atoms in the {111} facet is 9, while $Z \sim 4 \ldots 5$ may be reasonable for a rough surface. If so, the mobility of liquid Pb inclusions in Al in the high-temperature region may be controlled by the detachment of Al atoms from the rough surface of the Al matrix and in the low-temperature region by their detachment from {111} facets. This assumption does not contradict available data on the morphological behavior of Pb inclusions in an Al matrix which are given shortly below.

The equilibrium shape of solid Pb inclusions in Al is a cuboctahedron with atomically flat {100} and {111} facets, Fig. 16a [6]. Melting of Pb inclusions in Al is accompanied by rounding of the {100} facets while larger liquid inclusions retain flat {111} facets up to temperatures of 700 K and higher, Fig. 16b [7]. The temperature of this roughening process is size dependent. It could easily be anticipated to take place at 650 K for the 12 nm inclusion studied.

Thus, in the kinetic regime in the low-temperature region the higher activation enthalpy obtained from the Arrhenius plot may be related to the existence of {111} facets on the surfaces of liquid Pb inclusion. If this assumption is valid, i. e. that the transition in the Arrhenius plot is caused by the faceting of the inclusions, then, a detailed study of diffusion of inclusions may give the an alternative and possibly more accurate possibility of determining the temperature of the roughening and faceting transformations on their surface. Besides, our studies show that the liquid inclusions in the solid matrix are mobile at elevated temperature, therefore their observed shape can be distorted because of their motion.

7. Resume

Motion of free nanosized liquid Pb inclusions and inclusions trapped by dislocations in thin aluminum foils is studied using in-situ TEM. Liquid Pb inclusions attached to dislocations show random oscillations localized in the vicinity of the dislocation line. This is due to effect of the elasticity of dislocations on the trapped inclusions. Free inclusions move randomly along non-localized trajectories before they disappear on free surfaces or coalesce with other inclusions.

The model for kinetic behavior of particles attached to dislocations considered as an elastic string is developed. It is shown that the transverse and longitudinal motion of the particles are only weakly coupled and that they can be considered separately. The expression for the density of the distribution of positions of the particle on a dislocation line is

derived. The mathematical relations for the effective force constants and standard deviations are obtained for the transverse and longitudinal motion of the particle. They are in a reasonable agreement with the experimental values.

The diffusion coefficients are determined by Einstein's equation for motion of free inclusions, and Smoluchowski's equation are applied to estimate diffusion coefficients using transverse and longitudinal motion of trapped inclusions. The agreement between the diffusion coefficients of free and trapped inclusions indicates that it is the same microscopic mechanism that is responsible for their motion, possibly perturbed by a weak effect of the dislocations.

The dependence of the diffusion coefficient of the inclusions on their size indicates that the mobility is controlled by kinetic processes at the Al/Pb interface, e. g. diffusion along the Al/Pb interface in the diffusion regime and dissolution of the crystalline Al-matrix in the kinetic regime.

It is assumed that the low-temperature activation enthalpy of diffusion of the inclusion (3.05 eV) is related to the detachment of Al atoms from {111} facets of Pb/Al interface, and the high-temperature activation enthalpy (1.60 eV) corresponds to detachment of Al atoms from the rough Pb/Al interface. Then, the transition region (around 650 K) is associated with the appearance of the {111} facets of the inclusions.

We congratulate Prof. Shvindlerman with his lifelong contributions to the physics of materials and thank him for his constant interest to our studies and fruitful and stimulating discussions. The work was supported by the Director, Office of Basic Energy Sciences, Materials Science Division, US Department of Energy, under contract DE-AC3-76SF00098, the Danish Natural Sciences Research Council, and the Russian Foundation for Basic Research (Contract 05-03-33141). We are grateful to P. Ochin and his group (CNRS-CECM) for providing rapidly solidified materials.

References

[1] Y.E. Geguzin, M.A. Krivoglaz: Migration of macroscopic inclusions in solids, Consultants Bureau, New York (1973).
[2] G.A. Cottrell: Fusion Eng. Design 66–68 (2003) 253.
[3] G. Gottstein, L.S. Shvindlerman: Grain boundary migration in metals, CRC Press, Boca Raton a.o. (1999).
[4] K.N. Tu, J.W. Mayer, L.C. Feldman: Electronic thin film science. For electrical engineers and materials scientists, Macmillan Publishing Company, New York (1992).
[5] A. Christou (Ed.): Electromigration and electronic device degradation, John Wiley & Sons, New York (1993).
[6] E. Johnson, A. Johansen, U. Dahmen, S. Chen, T. Fujii: Mater. Sci. Eng. A 304 (2001) 187.
[7] H. Gabrisch, L. Kjeldgaard, E. Johnson, U. Dahmen: Acta Mater. 49 (2001) 4259.
[8] E. Johnson, H.H. Andersen, U. Dahmen: Microsc. Res. Techn. 64 (2004) 356.
[9] S. Prokofjev, V. Zhilin, E. Johnson, M.T. Levinsen, J.S. Andersen, U. Dahmen, T. Radetic, J.H. Turner, in: J. Čermák., J. Vřešt'ál (Eds.) Proc. VIII Seminar on Diffusion and Thermodynamics of Materials, Brno, Czech Republic (2002) 241.
[10] S.I. Prokofjev, V.M. Zhilin, E. Johnson, M. Levinsen, U. Dahmen, in: V.P. Ginkin (Ed.), Proc. 5th Int. Conf. Single Crystal Growth and Heat & Mass Transfer, Vol. 2, Obninsk, Russia (2003) 487.
[11] E. Johnson, J.S. Andersen, M.T. Levinsen, S. Steenstrup, S. Prokofjev, V. Zhilin, U. Dahmen, T. Radetic, J.H. Turner: Mater. Sci. Eng. A 375 (2004) 951.
[12] E. Johnson, M. Levinsen, S. Steenstrup, S. Prokofjev, V. Zhilin, U. Dahmen, T. Radetic: Phil. Mag. 84 (2004) 2663.
[13] S. Prokofjev, V. Zhilin, E. Johnson, M.T. Levinsen, U. Dahmen: Def. Diff. Forum 337 (2005) 1072.
[14] A.J. McAlister: Bull. Alloy Phase Diagrams 5 (1984) 69.
[15] M. Smoluchowski: Bull. Int. de l'cad. de Cracovie, Serie A (1913) 418.
[16] S.I. Prokofjev, V.M. Zhilin, E. Johnson: To be submitted.
[17] E. Johnson, S.I. Prokofjev, V.M. Zhilin: Unpublished data (2003).
[18] J.P. Hirth, J. Lothe: Theory of dislocations, McGraw-Hill, New York (1968).
[19] D. Gerlich, E.S. Fisher: J. Phys. Chem. Solids 30 (1969) 1197.
[20] C.J. Smithells, E.A. Brandes (Eds.): Metal Reference Book, Butterworths, Boston (1976).
[21] M. Smoluchowski: Sitzungsber. Kais. Akad. Wissensch. Wien (IIa), 123 (1914) 2381.
[22] A. Einstein: Ann. d. Phys. 17 (1905) 549.
[23] A.A. Chernov, in: B.K. Vainshtein (Ed.), Modern Crystallography, Vol. 3., Springer, Berlin (1984) Chapter 1.
[24] R. Kelly: Phys. Stat. Sol. 21 (1967) 451.
[25] F.A. Nichols: J. Nucl. Mater. 30 (1969) 143.
[26] N.A. Gjostein, in: J.J. Burke, N.L. Reed, V. Weiss (Eds.), Surfaces and Interfaces, Vol. 1, Syracuse University Press, Syracuse (1967) 271.
[27] F. Sawanayagi, R.R. Hasiguti: Jpn. J. Inst. Met. 42 (1978) 1155.
[28] B.S. Bokstein, Ch.V. Kopetskii, L.S. Shvindlerman: Thermodynamics and kinetics of grain boundaries in metals, Metallurgiya, Moscow (1986) (In Russian).

(Received April 27, 2005; accepted July 19, 2005)

Correspondence address

Professor Erik Johnson
Nano-Science-Center
Niels-Bohr-Institute
University of Copenhagen
Universitetsparken 5, Bygning D, DK-2100 Copenhagen, Denmark
Tel.: +45 353 20464
Fax: +45 353 20460
E-mail: johnson@fys.ku.dk